Molecular Therapy
Oncology
Original Article

An oncolytic herpesvirus expressing a CXCR4 antagonist interferes with glioblastoma cells' stemness features and migration

Paolo D'arrigo,[1,6] Maxime Dubois,[1,6] Judit Sanchez Gil,[1] Cédric Lassence,[1] Alexandre Hego,[2] Benoit Brouwers,[3] Arnaud Lombard,[3,4] Bernard Rogister,[3,5] Virginie Neirinckx,[3] Marielle Lebrun,[1,7] and Catherine Sadzot-Delvaux[1,7]

[1]Laboratory of Virology and Immunology, GIGA-Immunobiology, University of Liège, 4000 Liège, Belgium; [2]GIGA-Cell Imaging Platform, GIGA, University of Liège, 4000 Liège, Belgium; [3]Laboratory of Nervous System Disorders and Therapy, GIGA-Neurosciences, University of Liège, 4000 Liège, Belgium; [4]Neurosurgery Department, CHR Citadelle, 4000 Liège, Belgium; [5]Neurology Department, University Hospital, 4000 Liège, Belgium

Glioblastoma (GBM) is one of the most aggressive brain tumors. Despite the standard therapy, the survival from diagnosis remains dramatically low, especially due to tumor recurrence. Glioblastoma stem-like cells (GSCs) have been implicated in this tumor relapse, e.g., based on their capacity to escape the tumor and to migrate through the brain via CXCR4-dependent mechanisms. CXCR4 regulates biological features associated with tumor progression, including self-renewal, migration, and radio resistance. Importantly, its expression correlates with severity and poor prognosis of several cancers including GBM. The CXCR4/CXCL12 pathway therefore appears as an interesting potential therapeutic target. We have generated an oncolytic herpes simplex virus (oHSV) expressing HA-P2G, a mutated form of CXCL12 previously described as a CXCR4 competitive inhibitor. We demonstrate that, *in vitro*, oHSV/P2G impairs human GSC stemness marker expression, self-renewal, and migration. In two orthotopic xenograft murine models, oHSV/P2G intratumor injection limits tumor growth through the brain parenchyma and GSC migration through the *corpus callosum*. The ability of P2G to interfere with major GSC features demonstrates the interest in considering oHSV/P2G as a promising new therapeutic approach for GBM patients.

INTRODUCTION

Glioblastoma (GBM) is one of the most malignant brain tumors. Despite aggressive standard therapy, consisting in surgical resection followed by radio and chemotherapy, the current overall survival is only 15–16 months from the diagnosis,[1] due to a high recurrence rate. Recurrent tumors usually display poor sensitivity to standard therapies and high infiltrative capacity.[2]

Several studies have identified glioblastoma stem-like cells (GSCs) as partially responsible for GBM aggressiveness and recurrence.[3] Identified for their self-renewal abilities and the expression of neural stem cell (NSC) markers, GSCs have also been linked with increased invasive properties. In an orthotopic xenograft murine model, GSCs have been shown to escape the tumor, to invade the subventricular zone (SVZ) via the *corpus callosum*, and to be resistant to radio- or chemotherapy in a CXCR4/CXCL12-dependent manner,[4,5] properties that have been confirmed in humans.[6,7] In addition, they maintain an immune-suppressive microenvironment that is beneficial for the tumor growth.[8]

C-X-C chemokine receptor type 4 (CXCR4) and its ligand "Stromal cell-derived factor 1" (SDF1, better known as CXCL12) activate signaling pathways able to sustain stemness, proliferation, survival, and migration of tumor cells but also angiogenesis and immune response modulation.[9] Most GSCs highly express CXCR4 and produce CXCL12, revealing an autocrine signaling loop.[10] CXCR4, which emerges as a new marker of GSCs, is over-expressed in many cancers including GBM, and its expression usually correlates with tumor aggressiveness.[11–13] In addition, NSCs in the SVZ have recently been shown to harbor cancer-driving mutations and to participate to recurrence in a CXCR4/CXCL12-dependent manner.[14] In a mouse model, NSCs harboring p53 and PTEN (phosphatase and tension homolog) mutations have indeed been shown to be able to migrate into the cavity created by the primary tumor resection, differentiate into Olig2+ oligodendrocyte progenitors, and form a recurrent tumor, all of which being dependent on the CXCR4/CXL12 pathway.[14]

Preclinical studies have shown that inhibition of CXCR4 is able to alter GBM characteristics of aggressiveness.[15,16] Recently, a systemic delivery of nanoparticles coated with an iRGD peptide and in which a CXCR4 antagonist (AMD3100 or Plerixafor) is encapsulated resulted in the inhibition of GBM growth and activation of an anti-tumor microenvironment, thus confirming the importance of the

Received 2 October 2024; accepted 29 October 2025;
https://doi.org/10.1016/j.omton.2025.201083.

[6]These authors contributed equally

[7]These authors contributed equally

Correspondence: Sadzot-Delvaux Catherine, Laboratory of Virology and Immunology, GIGA-Immunobiology, University of Liège, 4000 Liège, Belgium.
E-mail: csadzot@uliege.be

CXCL12/CXCR4 pathway as a therapeutic target.[15] Several other CXCR4 antagonists have been evaluated in clinical trials for the GBM treatment, showing promising results when combined with standard therapies.[17] Among the CXCR4/CXCL12 inhibitors, mutated forms of CXCL12 have been shown to efficiently antagonize CXCR4 signaling pathway. Crump et al. demonstrated that switching the second amino acid of CXCL12 from a Proline to a Glycine (for that reason, called "P2G" in this manuscript) allows the mutated cytokine to bind CXCR4 while acting as a potent antagonist.[18] The anti-cancer effect of P2G has been described in breast cancer and osteosarcoma murine models, with various impact on metastasis formation[19,20] but so far not in GBM.

Oncolytic herpes simplex viruses (oHSVs) represent one of the most promising anti-cancer tools in the evolving landscape of virotherapy. Deep knowledge of HSV genome and a relative flexibility for genetic modifications have led to the engineering of a triple-mutated generation of oHSVs that has demonstrated its safety and is currently involved in clinical trials for the treatment of different tumors, including GBM.[21,22] In 2021, the Japanese Pharmaceuticals and Medical Devices Agency conditionally approved the first oHSV treatment (Delytact, G47Δ) for adult GBM.[23] However, in many cases, oHSVs alone are not sufficient to counteract GBM malignancy. For this reason, they are either used as part of combination therapies or engineered to express a transgene that can enhance their anti-tumor activity, both approaches being promising avenues.

We have engineered an oHSV armed with P2G (called oHSV/P2G), which can replicate in the tumor and locally induce the production and secretion of P2G. This approach combines thereby the well-described effects of oHSV virotherapy with the inhibition of a crucial signaling pathway, while avoiding side effects of a systemic administration of a CXCR4 antagonist. The current study focuses on oHSV/P2G impact on both GSCs' self-renewal and migration abilities, two important intrinsic GBM properties linked with GSC functions. These features have been addressed both *in vitro* in human patient-derived GSCs and *in vivo* in two murine orthotopic xenograft GBM model.[4]

RESULTS

Human GSCs express CXCR4 and CXCL12 at various levels

Five patient GSC cultures derived from newly-diagnosed (T08, T013, T018, and GB138[24]) or recurrent GBM (T033) have been used in this study. Considering the heterogeneity of patient-derived GSCs, these cell lines have been characterized for their capacity to express both CXCR4 and its ligand CXCL12. Flow cytometry analysis revealed that, apart from T08 that is barely positive for CXCR4 expression, the other GSC lines express CXCR4 at different levels (Figure S1A), with a very high expression in GB138 and T033 cells. The amount of CXCL12 produced in the supernatant and measured by ELISA showed that GB138 and T033 cells highly express CXCL12 while T08 cells secrete CXCL12 at a very low level (Figure S1B). T013 and T018 cells express both CXCR4 and CXCL12 at an intermediate level. To demonstrate the dependency of P2G effect on CXCR4 expression, most *in vitro* experiments aiming to evaluate oHSV/P2G impact have been carried out in parallel on GB138 and T08 cells, which respectively express high and low CXCR4 levels.

oHSV/P2G can antagonize CXCR4 signaling

oHSV/P2G has been engineered as follows. P2G coding sequence, under the EF1α promoter, has been inserted in the ΔICP34.5/ΔICP6 herpes simplex virus 1 (HSV-1) backbone, just after the pICP6-EGFP coding sequence (fQuick, kindly provided by Prof. EA Chiocca, Brigham and Women's Hospital, Boston, MA, USA). Moreover, P2G gene has been flanked by the interleukin-2 (IL-2) signal peptide and hemagglutinin (HA)-tag coding sequence, to promote its secretion and allow its detection, respectively (Figure 1A). To ensure its replication in GSCs, U_S12 gene coding for ICP47, which interferes with peptide presentation, has been deleted in the oHSV backbone. This deletion places the U_S11 gene, normally expressing a late protein, under the control of the U_S12 promoter, allowing thereby its expression as an immediate-early protein, partly restoring the infectivity of the oncolytic virus.[25] All constructs were verified by PCR and sequencing.

Western blot (WB) analysis of oHSV- or oHSV/P2G-infected GB138 or T08 cells revealed that, as expected, oHSV/P2G infection led to the expression and secretion of HA-tagged P2G by both GSC lines (Figure 1B).

Quantification of HA-tagged P2G in the supernatant of oHSV/P2G-infected GB138 cultures confirmed that P2G-HA is increasingly secreted up to 48 h after infection (Figure 1C). Filtration (0.1 μm filter) of the supernatant, previously proved effective in removing the viral particles without affecting the proteins in the medium,[26] did not affect the amount of P2G-HA (* in Figure 1C), making it possible to evaluate P2G impact independently of the viral infection or virus-induced cell death. Importantly, the amount of P2G detected in the supernatant (±1 ng/10^6 GB138 cells) was in the same range as the amount of CXCL12, the endogenous ligand of CXCR4 (±0.6 ng/10^6 GB138 cells) (Figure S1B).

Insertion of P2G transgene into the oHSV backbone did not impair the capacity of the virus to replicate in human GBM (Figure S2A), and, importantly, oHSV or oHSV/P2G infection has a similar impact on cell proliferation (Figure S2B). Culture in the presence of oHSV- or oHSV/P2G-conditioned medium (cm) did not affect cell proliferation either (Figure S2C). Finally, cell death upon infection was similar with both viruses (Figure S2D).

CXCR4 activation by CXCL12 triggers intracellular pathways, whose activation can lead to the ERK (extracellular signal-regulated kinase) or STAT3 (signal transducer and activator of transcription 3) phosphorylation, in a G-protein-dependent or -independent manner, respectively.[27] To confirm that P2G can antagonize CXCR4 signaling pathway, GB138 cells have been cultured in the presence of non-infected (NI), oHSV-, or oHSV/P2G-conditioned media, and the levels of phosphorylation of ERK and STAT3 were evaluated by WB (Figure 2). The densitometric quantification indicated that, contrary to oHSV(cm), oHSV/P2G(cm) significantly impaired the

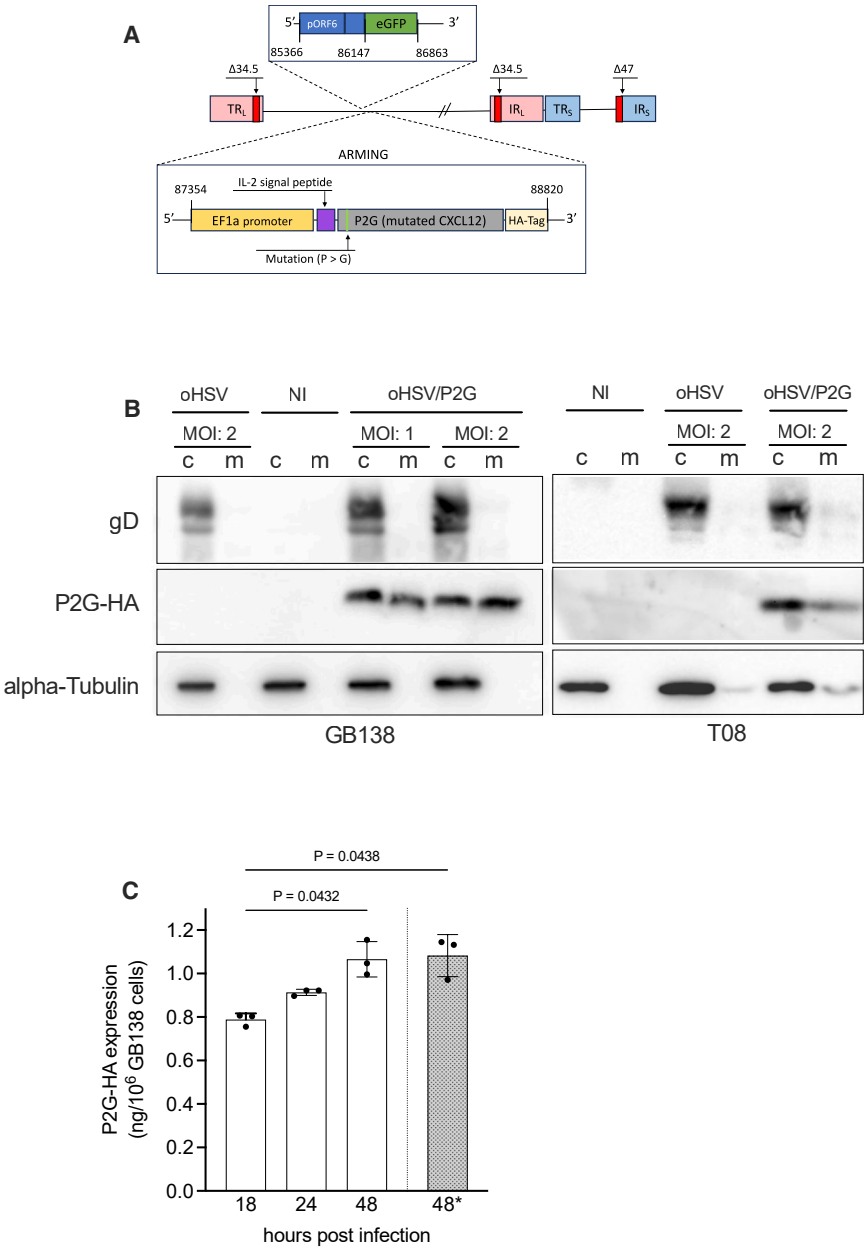

Figure 1. Construction and characterization of oHSV/P2G

(A) Schematic representation of oHSV/P2G genome. (B) P2G-HA expression by human GB138 (left panel) and T08 (right panel) primary cells was analyzed by western blot analysis performed on non-infected (NI), oHSV- or oHSV/P2G-infected cells lysates (c), and supernatant (m) (multiplicity of infection-MOI: 1 or 2). HSV glycoprotein D and α-tubulin detection were used as infection and loading control, respectively. (C) P2G-HA secretion in the supernatant was quantified by ELISA. Human GB138 cells were infected with oHSV or oHSV/P2G (MOI: 1), and the supernatant was harvested 18, 24, or 48 hours post-infection (hpi). In addition, the supernatant harvested 48 hpi was filtered to eliminate viral particle (0.1 μm filtration indicated by *). Bars represent the mean (SD) of 3 independent experiments. Statistical significance was determined by one-way ANOVA, with Tukey's multiple comparisons test with individual variances computed for each comparison.

phosphorylation of ERK, confirming the antagonistic properties of P2G on this signaling pathway. The phosphorylation of STAT3 followed the same trend with oHSV/P2G leading to a lower phosphorylation level of STAT3, but this effect was not statistically significant. AMD3100, a well-described CXCR4 inhibitor, led to decreased phosphorylation of both ERK and STAT3 without being statistically significant.

oHSV/P2G decreases GSC stemness marker expression and counteracts GSC self-renewal abilities

To investigate the effects of oHSV/P2G on GSCs key features, we first analyzed its impact on the expression of several markers, whose concomitant expression is generally linked to stem-like cell profile of GSCs.[28] Although oHSV infection of GB138 cells increased INTα6 and CD44 or decreased SOX2, OCT7, and SALL2 expression, oHSV/P2G infection led to a significant decrease of all these stemness markers' expression except for SALL2 expression, which decreased but not significantly (Figure 3A). Conversely, oHSV/P2G infection of T08 ($CXCR4^{low}$) cells had no significant effect on the expression of any of the analyzed stemness markers (Figure 3B). In line with these observations, infection of GB138 cells by oHSV/P2G significantly decreased the CD133 expression level compared to NI cells as analyzed by flow cytometry (Figure 3C).

The self-renewal ability of GB138 cells was then evaluated by either clonogenic or tumorsphere formation assays,[29] which respectively reflect the capacity of a single cell to form a colony by clonal expansion or to form spheres, two key features of GSCs. To limit the effect of the virus itself and to prevent virus-induced cell death from interfering with the observation of P2G effect, cells were infected at a low MOI (MOI: 0.1). The clonogenic assay revealed that, after 6 days of culture, the number of colonies was lower in the oHSV- or oHSV/P2G-infected cells than in the control condition, indicating that, despite the low MOI, the infection itself impairs the self-renewal capacity of GB138 cells, which nevertheless was even significatively more affected upon oHSV/P2G infection (Figure 3D).

To evaluate their capacity to form tumorspheres, GB138 cells were infected and cultured for 6 days in sphere-forming conditions.

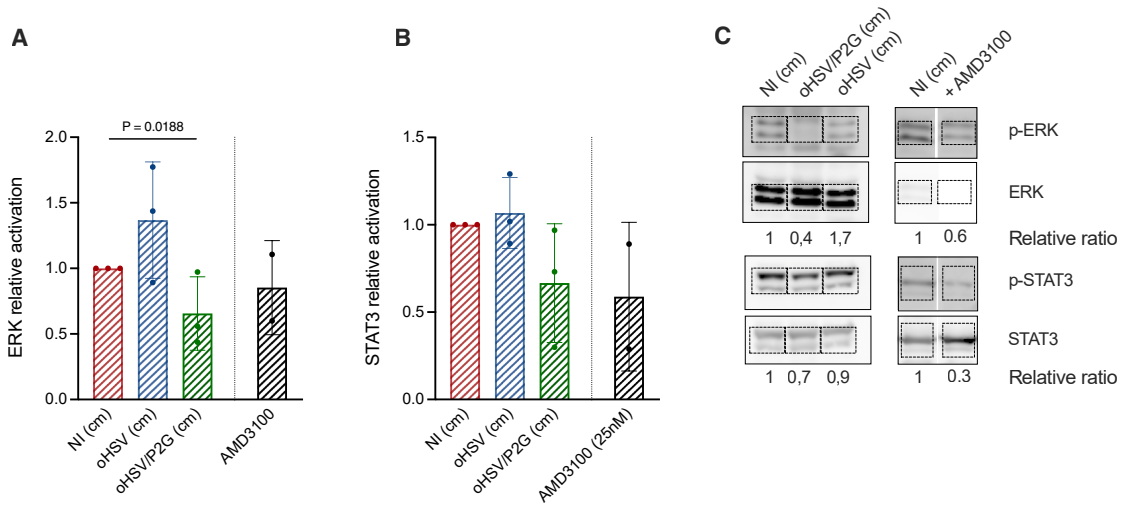

Figure 2. P2G impairs CXCR4 signaling pathway

P2G effect on CXCR4 signaling pathway was evaluated by western blot (WB) quantification of ERK (A) and STAT3 (B) phosphorylation in GB138 cells cultured with oHSV- or oHSV/P2G-conditioned media (cm) or AMD31000 (Plerixafor; 25 nM) used as a control of CXCR4 pathway inhibition. p-ERK/ERK and pSTAT3/STAT3 ratios were quantified by band densitometry after western blotting and expressed as the relative ratio with the ratio in cells cultured with NI(cm) considered as 1. Bars represent the mean (SD) of 3 independent experiments (2 for AMD3100). Statistical significance was determined by unpaired *t* test analyses. Representative pictures of a WB are shown in (C). Bands analyzed by densitometry for quantification are delineated by dotted lines.

Again, the infection itself had an impact on the capacities of GB138 cells to form tumorspheres, but the number of tumorspheres observed in oHSV/P2G-infected cells was even lower than that in oHSV-infected cells, demonstrating a significant effect of P2G itself (Figure 3E). This assay, repeated in the presence of conditioned media or AMD3100, confirmed that, contrary to oHSV(cm), which did not affect the tumorsphere formation, oHSV/P2G(cm) or AMD3100 significantly impaired the number of tumorspheres as compared to NI(cm) (Figure 3F). Interestingly, no significant difference was observed between oHSV/P2G(cm) and AMD3100 ($p = 0.958$). These results were confirmed for the other GSCs, except for T08 ($CXCR4^{low}$) cells for which a slight but not significant decrease was observed upon oHSV/P2G infection (Figure 3G).

oHSV/P2G counteracts GSC migration *in vitro*

Another important feature of GSCs previously observed *in vivo* is their capacity to escape the tumor mass and to migrate to a stem cell niche by a CXCR4/CXCL12-dependent mechanism. The migration of GSCs can be observed in the *corpus callosum,* through which they can eventually reach the SVZ.[4,30] This invading capacity of GSC is pointed as one of the mechanisms underlying GBM recurrence. The capacity of oHSV/P2G to impair GSC migration was first evaluated *in vitro* by transwell or sprouting assays.

GB138 tumorspheres were infected for 18 h with oHSV or oHSV/P2G (MOI: 0.1) before being dissociated and seeded onto laminin-coated transwells. Counting of cells that had migrated throughout the membrane over a 48 h period showed that the capacity of GB138 cells to invade the membrane was significantly impaired upon oHSV/P2G infection (Figure 4A left and middle panels). This observation was confirmed by quantification of the crystal violet released after lysis of cells that have migrated through the membrane (Figure 4A, right panel). In line with these results, the invasion ability of GB138 cells, cultured with oHSV/P2G(cm) or with AMD3100, was significantly lower than that in the presence of NI(cm) or oHSV(cm) (Figure 4B).

To confirm the ability of oHSV/P2G to impair GSC migration, sprouting assays were performed with T013 ($CXCR4^{medium}$) and T08 ($CXCR4^{low}$) tumorspheres previously infected or not with oHSV or oHSV/P2G. Twenty-four hours after seeding, migration of T013 cells was clearly impaired by oHSV/P2G infection while the effect on T08 cells was very limited (Figures 4C and 4D). Sprouting assay performed on cells cultured with conditioned media or media supplemented with AMD3100 confirmed these observations (Figures 4E and 4F). Although oHSV(cm) increased T013 cell migration, the presence of P2G significantly decreased it. AMD3100 tended to impair T013 cell migration as well, but its effect was not significantly different when compared to NI ($p = 0.167$) (Figure 4E). Conversely, migration of T08 cells was not affected neither by P2G nor by AMD3100 (Figure 4F). In these two assays, effects of P2G and AMD3100 were not significantly different.

Finally, both the transwell and the spouting assays were repeated in the presence of purified CXCL12 or AMD3100. In GB138 and T013 cells, CXCL12 significantly increased cell migration whereas AMD3100 tended to decrease it although its effect was not significant when compared to non-treated cells. On the contrary, CXCL12 or AMD3100 had no effect on T08 cells, confirming that GSC migration depends on the CXCR4/CXCL12 signaling (Figure S3).

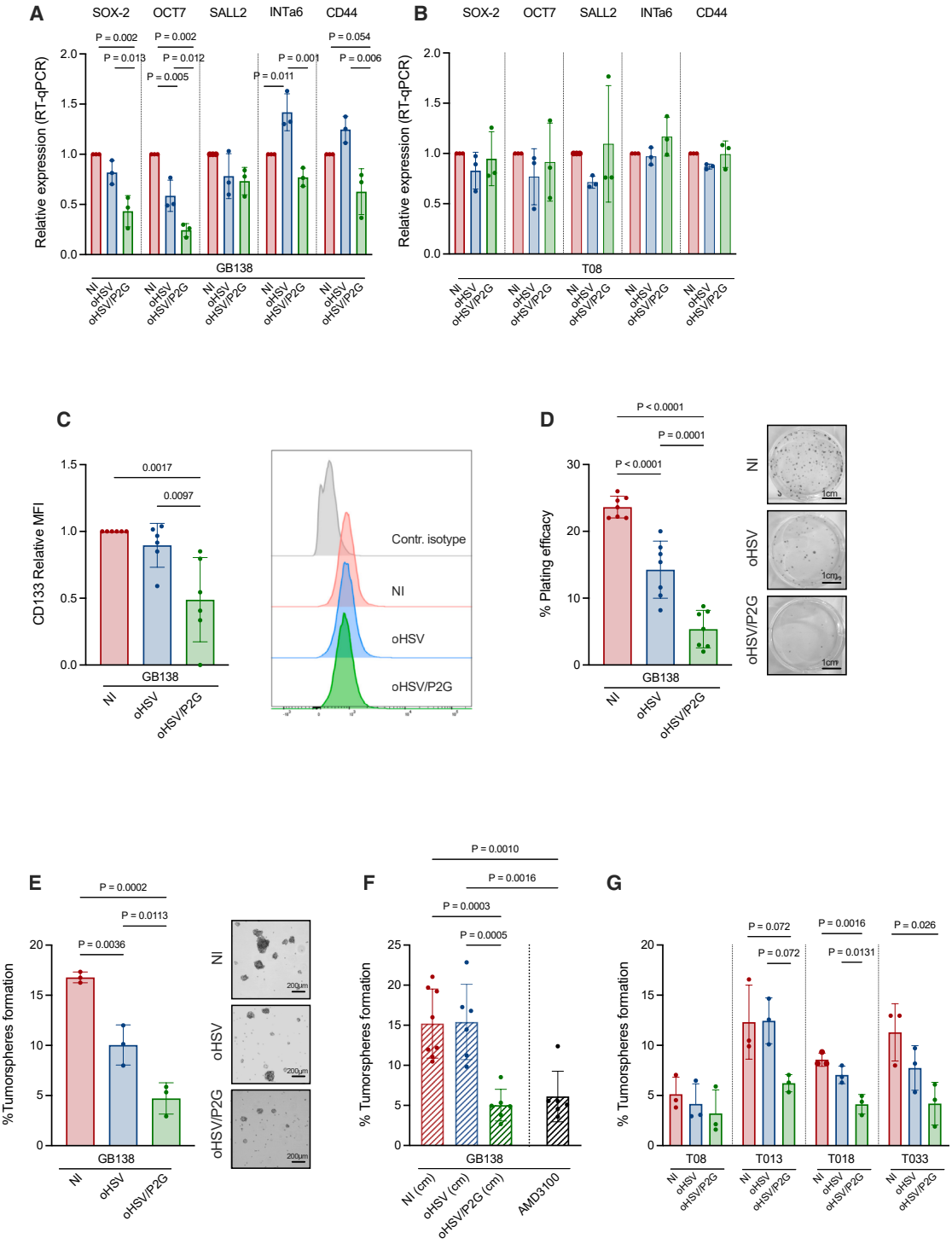

Figure 3. oHSV/P2G impacts stemness marker expression and GSC capacity to self-renew and to form tumorspheres

(A–C) Human GB138 (A and C) or T08 (B) cells were cultured as tumorspheres and infected with oHSV or oHSV/P2G (MOI: 0.1). Expression of stemness markers (SOX2, OCT7, SALL2, INTα6, and CD44) was evaluated 6 days post-infection by RT-qPCR and expressed relative to the level of expression in non-infected cells considered as 1 (A and B). Bars represent the mean (SD) of 3 (RT-qPCR) independent analyses. Statistical significance was determined for each gene by ordinary one-way ANOVA with Tukey's multiple comparisons test, with a single pooled variance. In parallel, GB138 cells were dissociated, and the median fluorescence intensity (MFI) of cells expressing CD133 at the plasma membrane was evaluated by flow cytometry (C). The MFI of 6 independent experiments is shown as relative to the MFI in the NI cells considered as 1 for each

(legend continued on next page)

oHSV/P2G impairs tumor growth and GB cell migration *in vivo*

The capacity of oHSV/P2G to interfere with tumor development and tumor cell migration was evaluated *in vivo* in two orthotopic xenograft murine models, with engraftment of GB138-RFP$^+$Luc$^+$ (Figure 5) or T033-LRLG (dsRed$^+$) (Figure 6), two GSC lines modified to express fluorescent marker.

A first experiment (Exp1) was performed in the GB138 model. For technical reasons, this experiment has been performed in two times with nine (3 in each experimental group) and twenty mice (6 for PBS or oHSV and 8 for oHSV/P2G treatments) (Figure 5A). Briefly, GB138-RFP$^+$Luc$^+$ cells were engrafted into the right striatum of *nude* mice (day 0). On day 19, *in vivo* bioluminescence imaging was performed to monitor tumor growth. Statistical differences between experimental groups were analyzed by R to take into consideration the potential bias resulting from pooling two independent sets of data (R script in supplemental material) and showed that all groups harbor a comparable bioluminescence signal intensity, without reaching statistical significance (Figure 5B). On day 20, PBS, oHSV, or oHSV/P2G (1×10^6 plaque-forming units [PFUs], 2 μL) was injected into the tumor mass. Mice were sacrificed on day 47, and brains were cleared for light-sheet microscopy analysis. The tumor volume estimation after 3D reconstruction clearly indicated that tumors in the oHSV- and oHSV/P2G-treated mice were smaller than those in the PBS group although the differences were not statistically significant (Figure 5C, statistical analysis in supplemental material). Importantly, while all PBS- or oHSV-treated mice harbored tumors, two oHSV/P2G-treated mice did not present any tumors at the end of the experiment.

After manual annotation of individual serial light-sheet images, the *corpus callosum* was 3D-reconstructed (representative pictures on Figure 5D; all pictures in Figure S4; exemplative 3D reconstruction in Video S1). Although tumors remain quite compact and did not invade the healthy surrounding tissue, we identified GBM cells escaping the tumor mass and migrating through the *corpus callosum*, in line with previous studies. These cells were highlighted using fire statistical colors, reflecting migration distance relative to the tumor axis, and the volume of the infiltrative tumoral tissue was measured. While migrating cells were observed in all PBS-treated tumors, they were observed in 66% of the oHSV- and only in 44% of the oHSV/P2G-treated groups (Figures 5E and S4). Moreover, the volume corresponding to cells migrating toward the *corpus callosum* was extremely low in oHSV- or oHSV/P2G-treated mice and significantly lower in oHSV/P2G-treated mice than in the control group (Figure 5F). The decrease of migration was even more marked considering the ratio between the volume of migrating cells and the whole tumor volume (Figure 5G), showing a clear and significant decrease in oHSV/P2G mice compared to control mice.

To evaluate the capacity of oHSV or oHSV/P2G to limit tumor growth, a long-term experiment was then performed in the same GB138 model (Exp 2). Briefly, 28 mice were engrafted with GB138-RFP$^+$Luc$^+$ cells and treated twice (day 20 and 42) with PBS (9 mice), oHSV (9 mice), or oHSV/P2G (10 mice) (Figure 5A). By day 139, none of the mice in any of the experimental groups had died nor exhibited abnormal behavior that would have warranted euthanasia. Mice were then sacrificed, and immunostaining on serial brain sections was performed to evaluate tumor size (Figures 5H and 5I). While most tumors of the PBS-treated mice were massive, some of them occupying almost the entire hemispheres, tumors in mice treated with oHSV or oHSV/P2G were either completely absent (3/9 and 4/10 in oHSV- and oHSV/P2G-treated mice, respectively) or very small, demonstrating the basal effect of virotherapy on the tumor growth. At this long-term experiment, no significant difference in tumor volume was observed between oHSV and oHSV/P2G, 139 days post-infection.

The capacity of oHSV/P2G to interfere with tumor development and tumor cell migration was also assessed in a more invasive T033-LRLG model.[31] As a prerequisite, we confirmed that T033 cells, isolated from a recurrent tumor and expressing CXCR4 at a high level, were able to migrate *in vitro* and that this migration was impaired upon oHSV/P2G infection (Figure S5A).

Mice were then engrafted with T033-LRLG cells expressing dsRed. Based on the tumor growth observed in previous experiments, PBS, oHSV, or oHSV/P2G (5 mice in each group) was administered by intratumor injection on day 14 and 21 from the engraftment (Figure 6A). One mouse did not receive any treatment and was considered as a control to evaluate the invasiveness of the T033-derived tumor about 2 months after engraftment (day 63). At this late time point, tumor cells were observed invading not only the right hemisphere in which the engraftment was done but also the left hemisphere, which was invaded mainly through the corpus callosum (Figure 6B, left panel). Tumor cells were detected on 8 serial sections (covering the distance from −2 to +2 mm around the bregma on the antero-posterior axis) confirming the capacity of T033-LRLG cells to

experiment (C, left panel), and histograms of a representative sample analysis are shown (C, right panel). Statistical significance was determined by ordinary one-way ANOVA with Tukey's multiple comparisons test, with a single pooled variance. (D) The capacity of GB138 cells to self-renew upon oHSV or oHSV/P2G infection (MOI: 0.1) was measured by a clonogenic assay. Bars represent the mean (SD) of 7 wells (3 independent experiments; 1 to 3 wells/condition in each experiment). Statistical significance was determined by one-way ANOVA with Tukey's multiple comparisons test, with a single pooled variance. A representative picture of each experimental condition is shown in parallel. Scale bar represents 1 cm. (E–G) The capacity of GB138 cells to form tumorspheres upon oHSV or oHSV/P2G infection was expressed as a percentage of plated cells forming spheres 18 h after plating. Representative pictures of tumorspheres upon mock (NI), oHSV, or oHSV/P2G infection are shown in parallel. Scale bar represents 200 μm (E). The experiment was repeated with GB138 cells cultured in the presence of NI-, oHSV-, oHSV/P2G-conditioned media or NI media supplemented with AMD3100 (40 nM) (F). Finally, 4 other patient-derived primary GSCs (T08, T013, T018, and T033) were mock-infected or infected with oHSV or oHSV/P2G (G). Bars represent mean (SD) of 3 (E and G) or 6 (F) independent analyses. Statistical significance was determined by one-way ANOVA with Tukey's multiple comparison test with a single pooled variance.

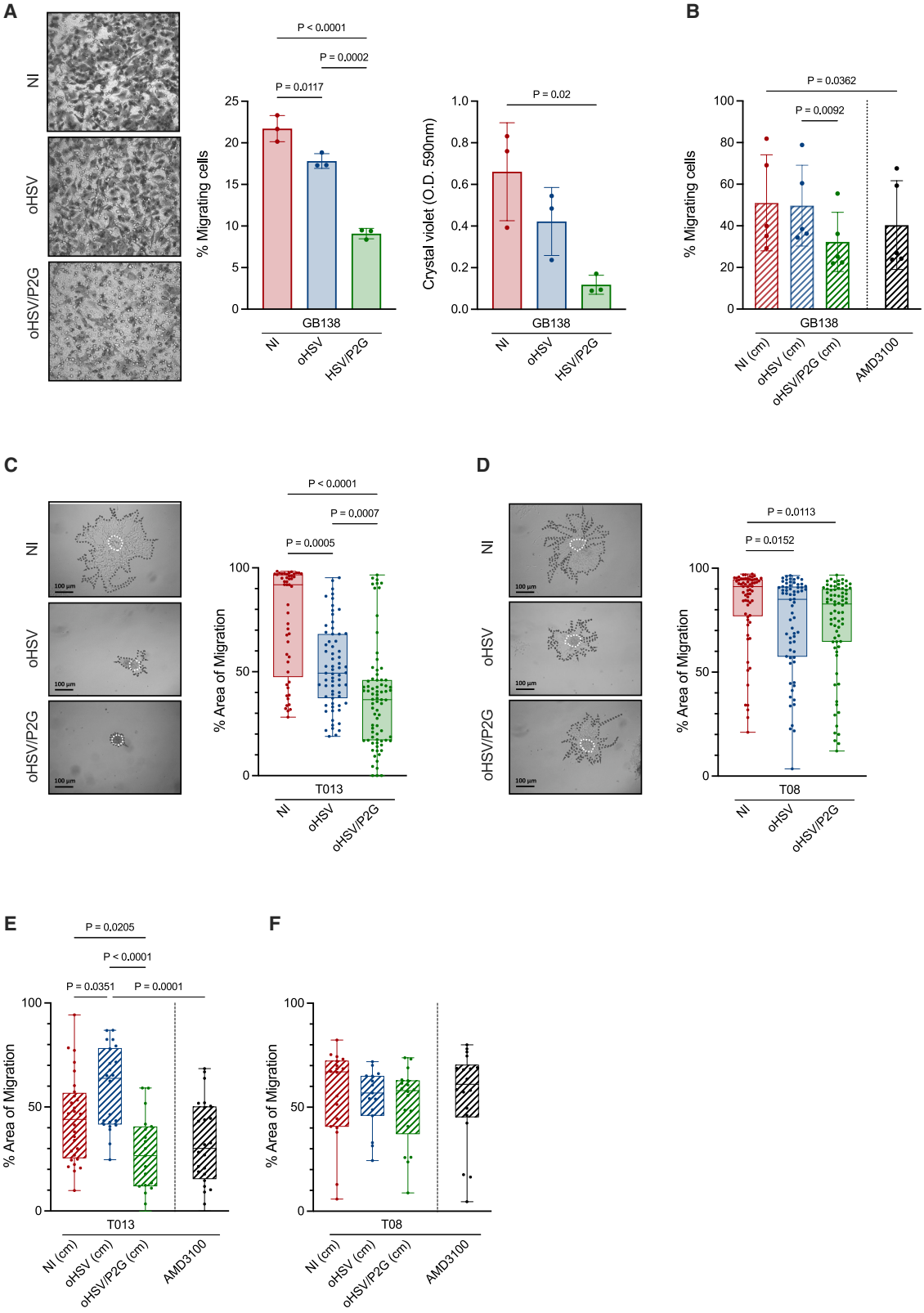

(legend on next page)

invade the whole hemisphere and to form a highly invasive tumor (Figures 6D and S5B, gray bar).

Analyses of the area of dsRed^{+} cells on each section using a machine learning-based pixel classifier revealed that the tumor area was significantly smaller in mice treated with oHSV or oHSV/P2G (Figures 6D and S5B) compared to PBS.

Quantification of the mean distance between the centroids of all annotated grid elements revealed that the capacity of tumor cells to migrate and infiltrate the surrounding healthy tissue was significantly reduced upon oHSV/P2G injection compared to PBS and to oHSV alone (Figures 6E and S5C), which highlights the interest of arming the virus with a CXCR4 inhibitor. Importantly, beside the basal effect of the virotherapy, which limits tumor size, arming the virus with P2G has a strong impact on cell migration, allowing to maintain the tumor in a more spatially defined area. These results were in line with the observations made in the GB138 model.

DISCUSSION

GBM is the most aggressive form of adult brain cancer and remains associated with poor prognosis mostly due to therapeutic failure and recurrences.[1] GSCs that express stemness markers, display strong self-renewal abilities, and are generally resistant to most therapies have been identified as contributing to GBM recurrence.[32] Moreover, GSCs participate to the establishment of an immune-suppressive microenvironment sustaining tumor growth.[8] As shown in previous studies, some GSC features such as self-renewal and capacity to form tumorspheres or to migrate are mediated by the CXCR4/CXCL12 pathway.[10,11,33] In many cancers including GBM, CXCR4 expression is correlated with poor prognosis, highlighting its inhibition as a potential therapeutic strategy.[12,13] Numerous preclinical studies have investigated the efficacy of systemic delivery of CXCR4 inhibitors with encouraging outcomes. However, systemic administration of CXCR4 inhibitors leads to side effects and poor pharmacokinetics properties.[34]

In addition to the side effects that can result from a systemic administration of any drug, the blood-brain barrier (BBB) further complicates the targeting of brain tumors. Therefore, many technical approaches are being considered to either allow the drug to be transported by a carrier capable of crossing the BBB or deliver the drug directly to the tumor.

A very promising technical approach is the use of nanoparticles to deliver drugs that can target either the tumor itself or the microenvironment and the immune cells in particular.[35] Synthetic protein nanoparticles coated with a cell-penetrating iRGD peptide and encapsulating small interfering RNA against STAT3, a major transcription factor associated with GBM progression, AMD3100, or immune checkpoint inhibitor have proven their efficacy to inhibit GBM proliferation to modify the microenvironment and to sensitize the tumor to radiotherapy.[15,36,37] Although able to cross the BBB upon systemic delivery, which constitutes an important step, nanoparticles were detected in various organs and in the liver in particular,[36] potentially leading to side effects, depending on the drug. More recently, extravesicular vesicles shown to play a role in various pathogenesis including cancer have been evaluated for their capacity not only to be loaded with drugs but also to be modified to specifically target a cell or a tissue. Although very novel and requiring deeper characterization, this approach using extravesicular vesicles derived from mesenchymal stem cells has been shown to cross the BBB more easily than synthetic nanoparticles and to be less immunogenic and appear thus as promising.[38]

Virotherapy and in particular herpes simplex virus virotherapy, which has proven its safety for GBM treatment, constitutes another powerful approach to ensure a localized administration while limiting the side effects on other organs. Many oHSVs have been developed to treat GBM and to target GSCs.[22] Many of those have been armed with transgene coding for cytokine, chemokine, cytotoxic, anti-apoptotic, anti-angiogenic transgene that will interfere with one or several biological processes involved in the tumor development. With their capacity to replicate in tumor cells and kill them while sparing healthy cells, they directly participate in the tumor size decrease. In addition, independently of the transgene, they can trigger the local and systemic immune response, which plays a crucial role in controlling the tumor.

We have engineered an oncolytic HSV-1 (Δγ34.5/ΔICP6/ΔICP47) armed with a mutated form of CXCL12 (called P2G) described in

Figure 4. oHSV/P2G impacts GB cell migration

(A and B) Transwell assay: GB138 cells infected or not with oHSV or oHSV/P2G (MOI: 0.1) were cultured in the upper insert of a two-compartment culture device (Transwell), and their capacity to migrate through the transwell membrane was evaluated after 48 h. Representative picture of each condition is shown in the left panel (magnification: 20x) while migration is represented either as the percentage of cells that have migrated through the transwell membrane (middle panel) or by the measure of the crystal violet released after the lysis of cells that have migrated (right panel) (A). The same experiment was performed with cells cultured in the presence of non-infected (NI), oHSV- or oHSV/P2G-conditioned media (cm), or NI-conditioned media supplemented with AMD3100 (40 nM) (B). Bars represent the mean (SD) of 3 (A) or 5 (B) independent experiments. Statistical significance was determined by one-way ANOVA, with Tukey's multiple comparisons test, with individual variance computed for each comparison. (C–F) Sprouting assay: T013 (CXCR4^{medium}) (C) and T08 (CXCR4^{low}) (D) GSCs cultured as tumorspheres were either non-infected or infected with oHSV or oHSV/P2G. Representative pictures are shown in parallel (left panels). The sphere areas were measured at 1 hpi (hours post-infection, white dotted lines) and 24 hpi (dark dotted line), and the percentage of migration (right panels) was expressed as follows: (*Total area at 24h-Area at 1h*)/*Total areaat 24h*. Scale bar represents 100 μm. The same experiment was repeated with T013 (E) or T08 (F) cells cultured with NI-, oHSV- or oHSV/P2G-conditioned media or NI-conditioned media supplemented with AMD3100 (40 nM). Boxplots represent the repartition of the values of each dataset, each dot representing one sphere. Area of migration has been measured in 4 (C and D) or 3 (E and F) independent experiments. Whiskers represent the maximum and minimum values. Statistical significance was determined by Kruskal-Wallis test (C and D) or ordinary one-way ANOVA (E and F), depending on the normality evaluated with the Shapiro-Wilk normality test.

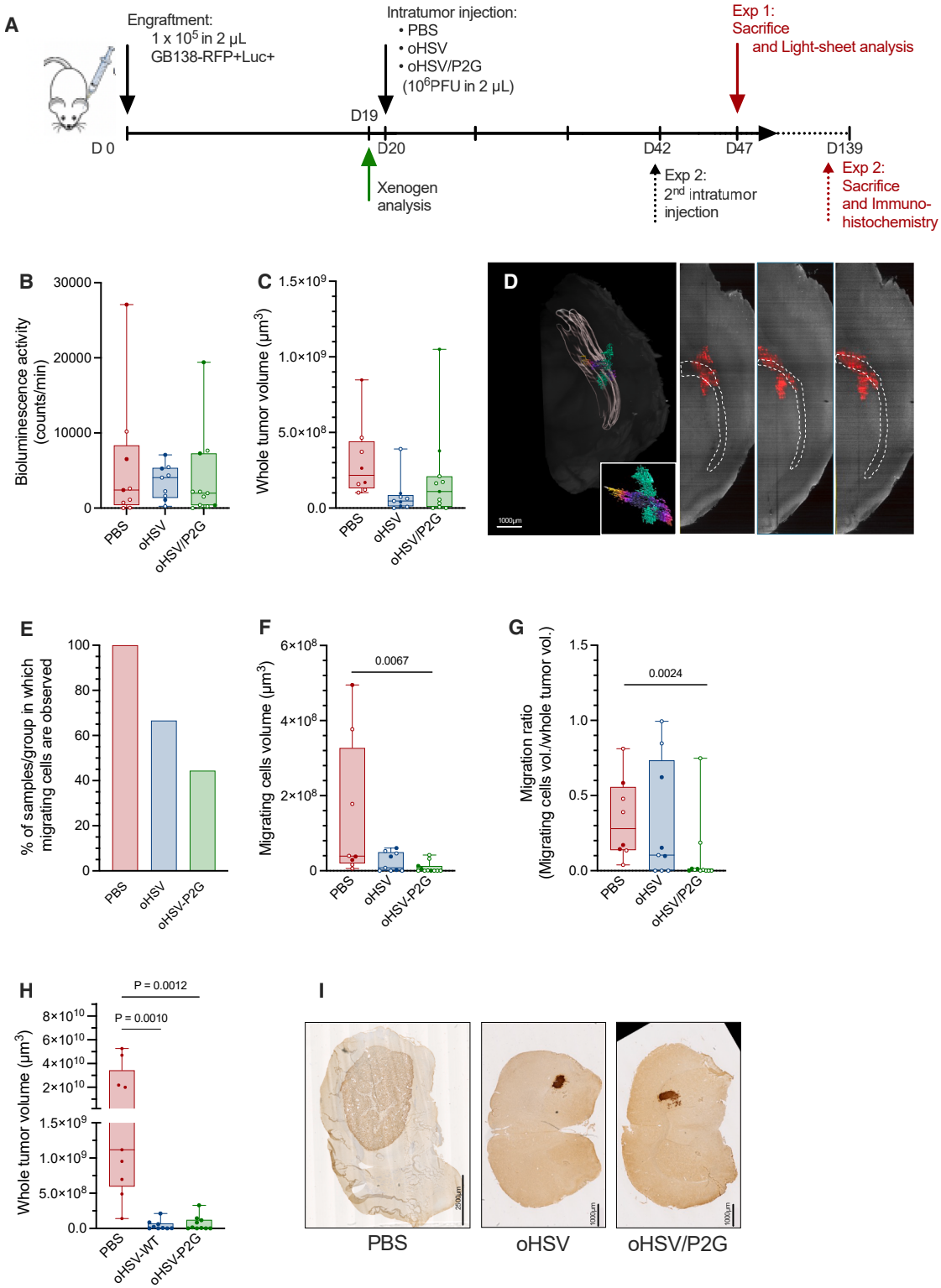

Figure 5. oHSV/P2G impairs GB cell migration in a GB138 cell orthotopic xenograft *in vivo* model

(A) Experimental settings of the orthotopic xenograft model. (B) to (G) correspond to Exp1 (short-term) results while (H) and (I) correspond to Exp 2 (long-term). (B) Size of the tumor evaluated by bioluminescence imaging on day 19. For technical reason, Exp 1 (B–G) was performed in two consecutive series, and two dataset were thus obtained

(legend continued on next page)

the literature as a potent CXCR4 inhibitor.[18] Considering that the CXCR4/CXCL12 pathway controls many biological mechanisms involved in cancer progression, we hypothesize that P2G might have a very broad effect not only on GBM cells, which are the focus of this work, but also on the microenvironment.

The insertion of P2G does not impair virus replication and leads to the secretion of P2G by the infected cells. Furthermore, the amount of P2G secreted by the infected GBM cells is shown to be similar to the amount of endogenous CXCL12.

Although the virus itself influences human GSC phenotype and even though arming does not induce additional cell death compared to the virus itself, the presence of P2G has a significant impact on GSC features as compared to the non-armed virus. Arming with P2G, indeed, significantly decreases stemness markers' expression and impairs self-renewal and migration capacities of GSCs as confirmed by culture with conditioned media devoid of viral particles. Importantly, the effect of P2G depends on the level of CXCR4 in patient-derived GSCs and is therefore very low in GSCs with low levels of CXCR4 expression.

In a GB138 orthotopic xenograft murine model, intratumor injection of either oHSV or oHSV/P2G reduces tumor size, as estimated by 3D-reconstructed light-sheet microscopy images and immunohistochemical staining. It should be noted that in Exp 1 (short-term experiment), one of the oHSV/P2G-treated mice harbors a huge tumor, comparable to the tumors usually observed in the PBS group. This could account for technical issues, in particular to the difficulties to ensure the virus injection into the tumors, which grow slowly and are very small at the time of treatment. Interestingly, while all PBS- or oHSV-treated mice developed a tumor, two (out of 11) oHSV/P2G-treated mice did not, as observed in light-sheet microscopy analysis carried out at the end of the experiment (day 47, Figure S4). Importantly, in a long-term experiment (Exp 2) in which mice were treated twice (3 weeks apart) and sacrificed about 100 days after the second treatment, tumors in the PBS group were huge, occupying a large part of the hemisphere while tumors in both oHSV- and oHSV/P2G-treated mice were very small and even undetectable in 33% (3 out of 9) and 25% (4 out of 10) in oHSV- and oHSV/P2G-treated mice, respectively. These observations demonstrate that virotherapy could lead to a long-lasting impact despite the absence of adaptive immune response in *nude* mice. Surprisingly, despite the size of the tumors, none of the PBS-treated mice lost weight or displayed abnormal behavior. However, for ethical reasons, all mice were sacrificed on day 139, and no survival assay was performed.

Although presenting GSC features and being able to migrate, GB138 cells lead to tumors that grow quite slowly and remain in a relatively defined region with tumor cells migrating quite exclusively through the corpus callosum. To confirm the capacity of oHSV/P2G to limit GSC migration, another *in vivo* model was thus set up. After only 2 months, T033 tumor cells were detected not only all over the right injected hemisphere but also in the left hemisphere, reflecting high invasiveness. Once again, both oHSV and oHSV/P2G were able to reduce tumor size.

Notwithstanding encouraging results demonstrating the capacity of oHSV/P2G to significantly impair stemness features *in vitro*, we could not demonstrate *in vivo* a clear-cut improvement upon oHSV/P2G treatment compared to non-armed oHSV regarding the capacity to kill the tumor cells and to clear the tumor *in vivo*. Considering that, *in vitro*, oHSV and oHSV/P2G lead to cell death with the same efficacy and impact similarly cell proliferation, it is not surprising that, *in vivo*, in absence of adaptive immune response known to play a critical role in the virotherapy efficacy, no significant differences of tumor size could be observed about 100 days after the viral injection. However, it is important to note that, while most *in vitro* experiments were performed with a low MOI (0.1), a high dose of virus (10^6 PFU) was injected in the tumor to ensure the virotherapy efficacy. Although impossible to evaluate, the MOI at the site of injection is thus probably much higher than that in *in vitro* experiments. We could not rule out that, *in vivo*, the viral infection itself has such a strong impact on tumor growth that the impact of P2G is underestimated. It would be worth evaluating whether a lower MOI would have a less drastic effect on the tumor size while sustaining a stronger and long-lasting production of P2G that would highlight its impact.

GSCs can escape the tumor in a CXCR4-dependent manner and migrate through the *corpus callosum*, potentially to the SVZ,[4,39] which could participate to treatment failure and recurrence. In

(plain dot: first series, circle: second series). Statistical significance (for B–G) was determined in R (R script available in supplemental material) to verify whether any bias might result from differences between the two datasets. (C) Whole tumor volume measured on tumor 3D reconstruction (Imaris) of brains recovered on day 47. Despite the trend showing a reduction of the tumor volumes in the oHSV and oHSV/P2G mice, no statistical difference with the control group was observed (R script available in supplemental material). (D) Representative picture of the 3D reconstruction of the tumor mass (green) and of cells migrating (statistically fire-colored according to their distance to the central tumor mass) through the *corpus callosum* (gray). Scale bar represents 1 mm. 3D reconstruction of the tumor mass and of migrating cells is shown independently of the *corpus callosum* in the insert. Three individual images of that specific sample are shown on the right panels. Cancer cells (RFP^+) and the *corpus callosum* (manually annotated) appear in red and white dotted lines, respectively. Pictures of Imaris 3D modelization of all brains are shown in Figure S4. A movie allowing to visualize the steps of the 3D reconstruction and to turn it at 360° is available in the supplemental information (Video S1). (E) Percentage of mice for which cells migrating through the *corpus callosum* were observed. (F and G) Volume of cells migrating through the *corpus callosum* (F) or ratio of migrating cells regarding the volume of the whole tumor (G). Boxplots represent the repartition of the measures carried out on 8 (PBS), 9 (oHSV), and 11 (oHSV/P2G) mice with whiskers representing the maximum and minimum values. (H and I) Long-term experiment (Exp 2). Whole-tumor volume of brains recovered on day 139 (H). Boxplots represent the repartition of the measures form 9 (PBS and oHSV) and 10 (oHSV/P2G) mice with whiskers representing the maximum and minimum values. Statistical significance was determined with a Kruskal-Wallis test after Shapiro-Wilk normality test. A presentative picture of one section is shown for each experimental group (I). Scale bar represents 2.5 mm (oHSV) or 1 mm (oHSV and oHSV/P2G).

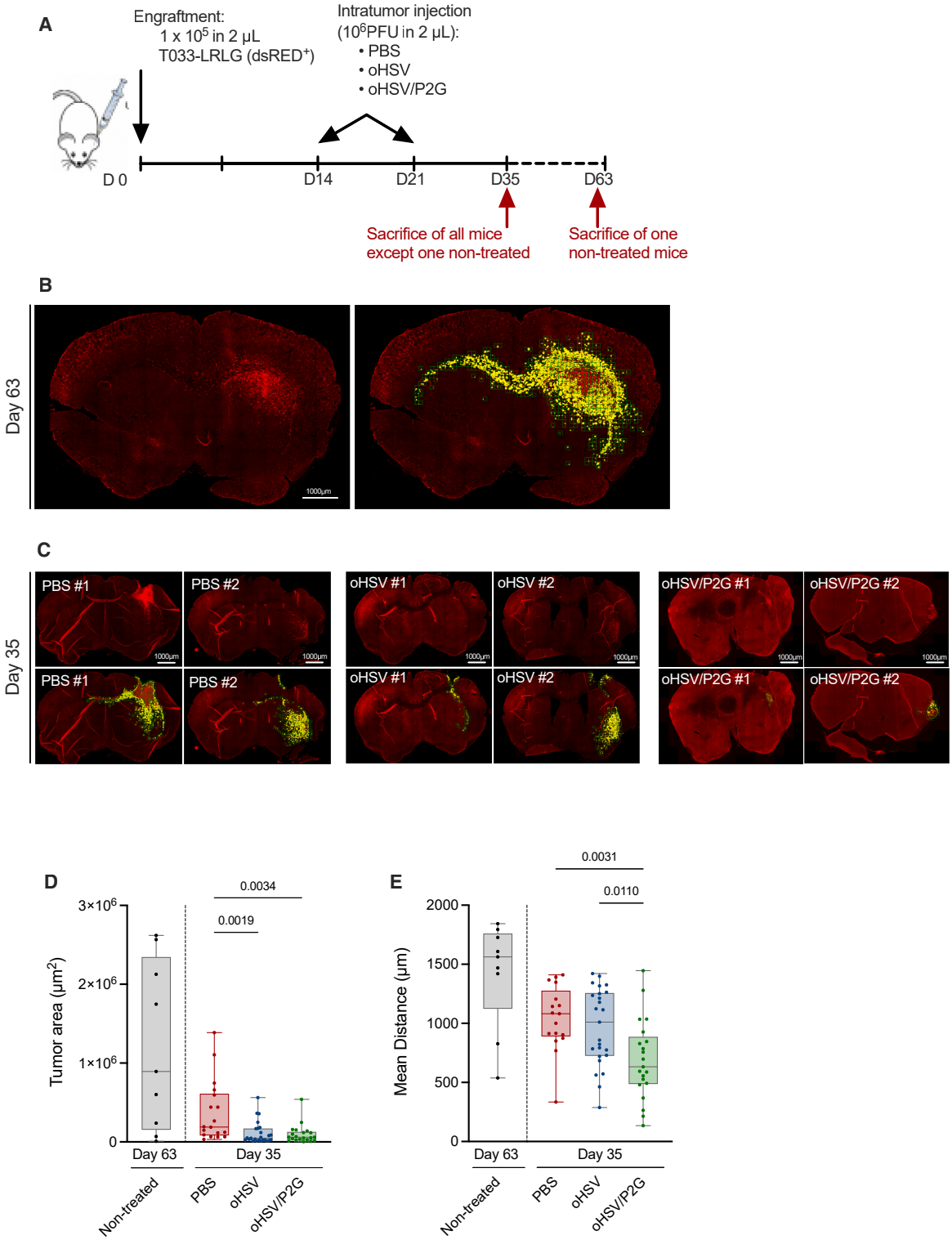

Figure 6. oHSV/P2G impairs GB cell migration in a T033 cell orthotopic xenograft *in vivo* model

(A) Experimental settings of the orthotopic xenograft model. (B) Representative picture of brain sections of the mice sacrificed on day 63 (non-treated mice). Images were with obtained with a Zeiss Axioscan 7 slide scanner (20× objective) (left panel) and analyzed for quantification (right panel). Scale bar represents 1 mm. Image analysis was

(legend continued on next page)

addition, CXCR4 is also involved in the differentiation of NSCs harboring cancer-driving mutations into Olig2$^+$ oligodendrocyte progenitors and of their migration into the cavity created by primary tumor resection where they can form a recurrent tumor.[14] It should therefore be considered that inhibiting cell migration by inhibiting CXCR4 could be beneficial, particularly by reducing the ability of tumor cells to give rise to recurrences. We clearly showed that P2G arming impairs cell migration, both *in vitro* and in two different *in vivo* models. Importantly, in the GB138 model, no tumor cell migration was observed in 5 mice (out of 9; 55%) in the oHSV/P2G group while observed in all PBS- and in 3 (out of 9; 33%) oHSV-treated mice. Moreover, considering the size of the tumors, cell migration was extremely limited in all oHSV/P2G samples. These observations were confirmed in the T033 model. In this model, which harbors more invading capacities, oHSV/P2G, in contrast to oHSV, significantly impaired tumor cell migration distance, resulting in less infiltrative tumors. These observations highlight the capacity of a CXCR4 inhibitor locally expressed by an armed oncolytic virus to restrain tumor cell migration. Impairing tumor cell migration is certainly of high interest, not only because it limits the capacity of the GSCs to reach the SVZ or other niche where they could hide and acquire treatment resistance[5] but also because consequently the tumor mass remains more compact, thereby facilitating the possibility of further surgical resection.

While the SVZ constitutes an important niche for GSCs, it is not the only niche where they can hide. Hira and colleagues have indeed shown that hypoxic peri-arteriolar tissue constitutes a GSC niche similar to the hypoxic peri-arteriolar hematopoietic stem cell niches[40] and that CXCR4 antagonists may mobilize GSCs from this niche and sensitize them to therapy.[41] Surgical resection and radiotherapy, considered as first-line treatment, are usually followed by vasculogenesis promoted by a CXCR4-dependent recruitment of bone marrow-derived cells (BMDCs), which can be inhibited by CXCR4 inhibitors. Although not investigated in the current study, it would really be worth investigating tumor vasculogenesis and mobilization of both GSCs and BMDCs, which would reinforce the rationale of oHSV/P2G administration after the current treatment.

Besides their capacity to lyse tumor cells, oncolytic viruses can also impact the tumor microenvironment (TME). They can trigger the production of cytokines and thereby recruit immune cells.[42–44] CXCR4 inhibitors have also been shown to reshape the TME and to potentiate immunotherapy in melanoma,[45] in ovarian cancer,[46] and in GBM.[37,47] In preclinical models, they have been shown to switch macrophages from a pro-tumor M2-like to an anti-tumor M1-like phenotype.[48] Of note, pro-tumoral macrophages, particularly abundant in GBM, correlate with faster progression and therapy resistance. In addition, CXCR4 inhibition has recently been shown to decrease regulatory T cells (Treg) recruitment, to impair their functions and more generally to counteract immunosuppressive properties of the TME.[49] It is thus crucial to evaluate the oHSV/P2G effect on the immune response. Characterization of oHSV/P2G in an immunocompetent syngeneic model will allow to confirm that, in GBM, CXCR4/CXCL12 inhibition not only modifies GSC phenotype and capacity to migrate but also modulates the TME, thereby controlling tumor growth as described for other cancers.

In conclusion, our results demonstrate that oHSV/P2G has a significant impact on GSCs, reducing their stemness marker expression and significantly impairing their self-renewal and migration capacity both *in vitro* and *in vivo*.

oHSV/P2G virotherapy, whose impact on CXCR4$^+$ cells of the TME needs to be further evaluated, could thus be considered as an add-on to the first-line treatment, to limit the risk of relapse and improve GBM prognosis.

MATERIALS AND METHODS

Cell lines

Vero cells (ATCC, #CCL-81) and patient-derived human GBM GB138 cells,[24] were maintained in Dulbecco's modified Eagle's minimal essential medium high glucose (DMEM HG, Lonza, Verviers, Belgium) supplemented with 10% fetal bovine serum (FBS). GBM patient-derived cultures (T08, T013, T018, and T033[24]) were established from residual tumor tissue after surgical resection (Neurosurgery department, Liège University Hospital -CHU- and University Hospital Biobank -BHUL-, Liège, Belgium), in accordance with the legal regulations on residual human body material. GB138 RFP$^+$ Luc$^+$ and T033-LRLG[31] cells expressing RFP and dsRed, respectively, were used for follow-up in *in vivo* experiments. All GSCs were cultured as tumorspheres in stem cell medium (DMEM/F12 with GlutaMAX [Gibco] supplemented with B27 [1/50] without vitamin A [Gibco], 1% penicillin-streptomycin [Lonza, Verviers, Belgium], 1 μg/mL of heparin [n 7692.1, Carl Roth, Belgium], recombinant human epidermal growth factor [20 ng/mL], and recombinant human

performed with QuPath using a machine learning-based pixel classifier to identify dsRed$^+$ signal (yellow pixels, right panel). A 100 × 100 μm grid was overlaid on each image, and only grid elements containing tumor annotations were retained for further quantification (green, right panel). (C) Pictures of brain sections from PBS-, oHSV-, or oHSV/P2G-treated mice (2 mice/experimental condition as representative example; day 35) and of the analysis performed for quantification (yellow: dsRed$^+$ signal detection; green: 100 × 100 μm overlaid grid). Scale bar represents 1 mm. (D) Tumor area estimated on each brain section from one non-treated or 5 PBS-, oHSV-, or oHSV/P2G-treated mice. Tumor area corresponds to the cumulative area of tumor cells detected in QuPath (yellow pixels). Boxplots represent the repartition of the values of each dataset, each dot representing the quantification on one slide. Tumor area estimated on each section from a single brain is represented in Figure S5B. Whiskers represent the maximum and minimum values. Statistical significance of day 35 data was determined by Kruskal-Wallis test after Shapiro-Wilk normality test. (E) Tumor cell spread estimated on brain sections from one non-treated or 5 PBS-, oHSV-, or oHSV/P2G-treated mice. Cell spread is estimated by the mean distances between the centroids of annotated grid elements. Boxplots represent the repartition of the values of each dataset, each dot representing the quantification on one slide. Mean distance estimated on each section from a single brain is represented in Figure S5C. Whiskers represent the maximum and minimum values. Statistical significance of day 35 data was determined by Kruskal-Wallis test after Shapiro-Wilk normality test.

fibroblast growth factor 2 [20 ng/mL] [Peprotech]). When indicated, GB138 were cultured as monolayers.

Construction of recombinant oHSVs

Recombinant viruses were engineered in fHsvQuik-1 bacterial artificial chromosome (BAC) containing an attenuated HSV-1 (strain F) (Δγ34.5, ΔUL39, GFP^+; kind gift from A. Chiocca, Brigham and Women's Hospital, Boston, MA, USA). Further ICP47 deletion was done as described by Todo et al.[50] Recombinants were obtained by the two-step Red recombination technique "en passant."[51] The sequence of human mutated CXCL12 sequence (second amino acid mutated P to G) flanked by the IL-2 signal peptide and HA tag in 5′ and 3′, respectively, and controlled by the EF1a promoter was inserted just after the EGFP gene (Figure 1A). Vero cells seeded in 6-well plates were transfected with this construct using jetPEI (Polyplus, Illkirch – FRANCE). Virus stocks were produced as previously described.[52] Viral particles were then ultracentrifuged, resuspended in PBS with 10% glycerol, and stored at −80°C. Virus titration was performed in Vero by plaque assay.[53]

Virus and cm production

GB138 cells were grown in DMEM HG 10% FBS. At confluence, the culture medium was removed and replaced by DMEM/F12 (without added growth factors), and cells were mock-infected or infected with oHSV or oHSV/P2G (MOI: 1). After 48 h, media were collected, centrifuged (260*g*, 5 min), filtered with 0.1 μm filter (Pall Life Sciences 4611 Acrodisc syringe filters with Supor membrane, 25 mm, 0.1 μm, sterile), aliquoted, and stored at −80°C.

Viral growth assay

50K GB138 cells were seeded in 24-well plate for 24 h and then infected with oHSV or oHSV/P2G (MOI 0.1 and 1). Virus replication was measured by recording GFP signal for 48 h (Incucyte S3). Total green object area (μm^2/well) was used to assess virus replication. Total object area measured with contrast imaging was recorded in parallel and expressed relative at T0 to evaluate the cell proliferation.

Detection of P2G-HA by WB

400K cells were seeded for 24 h before being infected with oHSV or oHSV/P2G (MOI: 1 or 2). Supernatant and cells were harvested 18 h post-infection (hpi).

Cells were lysed using modified RIPA buffer (Tris-HCl 50 mM pH 7.5, NaCl 150 mM, EDTA 1 mM, NP40 1%, and deoxycholate 0.25%) supplemented with proteases inhibitors (cOmplete, Roche).

Supernatants were diluted in acetone (1:4) to precipitate the proteins and further centrifuged at 13,000 rpm for 30 min.

After electrophoresis and transfer onto polyvinylidene fluoride membrane (GE Healthcare), membranes were incubated overnight at 4°C with anti-gD (ref. sc-21719, Santa Cruz; dilution 1:1,000), and anti-HA (ref. ab9110, Abcam; 1:1000) antibodies. Mouse anti-alpha-tubulin (ref. T6199, Sigma; 1:2,000) was used as loading control. HRP-conjugated anti-mouse immunoglobulin G (IgG) (ref. 7076, Cell Signal; dilution 1:2,500) or horseradish peroxidase (HRP)-conjugated-anti-rabbit IgG (ref. 7074, Cell Signal; 1:2,500) was used as secondary antibodies. After incubation with enhanced chemiluminescence (ECL) solution (luminol: 25 mg/100 mL in Tris-HCl pH 8.6 0.1 M; para-hydroxy coumaric acid 11 mg/10 mL DMSO; H_2O_2 35%), chemiluminescence signals were recorded with LAS4000 CCD camera (GE Healthcare).

pERK and pSTAT relative quantification

125K GB138 cells were seeded in T25 in stem cell culture medium. After 6 days, the culture medium was replaced by conditioned media supplemented with CXCL12 (80 pM) to induce CXCR4 signaling pathway. After 30 min, cells were harvested, lysed using modified RIPA buffer, and analyzed by WB with anti-ERK (#9102, Cell Signal; dilution 1:2,000), anti-pERK (#9106S, Cell Signal, 1:2,000), anti-STAT3 (#9139 Cell Signal, 1:1,000), or anti-pSTAT3 (#9145, Cell Signal, 1:1,000) antibodies. Mouse anti-alpha-tubulin (#T6199, Sigma; 1:2,000) was used as a loading control. HRP signals were revealed using ECL and imaged with LAS4000 CCD camera (GE Healthcare). Band densitometry was analyzed using ImageJ.

P2G-HA quantification by ELISA

P2G-HA quantification in the culture supernatants was performed by ELISA with the HA tag ELISA kit (ref MBS3802035, MyBioSource), according to the manufacturer protocol.

Resazurin assay

50K GB138 cells were seeded in 24-well plate for 24 h and then infected with oHSV or oHSV/P2G (MOI: 1). After 24, 48, or 72h, culture medium was removed, cells were washed with PBS, and medium were replaced by 300 μL of resazurin solution (1/5 resazurin +4/5 DMEM/F12). After 4 h, resazurin was transferred into a 96-well black opaque plate. Fluorescence was measured using FilterMax F5 multi-mode microplate reader and expressed as relative fluorescent units (Ex = 530–570 nm, Em = 590–620 nm).

RT-qPCR

Cells were seeded in 6-well plates (400K cells/well) for 24 h before being infected with oHSV or oHSV/P2G (MOI: 0.1) for 18 h and kept growing as tumorspheres.

Tumorospheres were then dissociated with Accutase (Biowest, Nuaillé, France), and 125K cells were seeded in T25 in stem cells medium. Six days after plating, the spheres were collected and total RNA was purified (Nucleospin kit, Macherey-Nagel, according to the manufacturer's protocol). One μg of RNA was reverse-transcribed using RevertAid H Minus First Strand cDNA Synthesis Kit (Thermo Scientific) with random primers. TATA-Box binding protein (TBP) transcripts or 18S rRNA were used as controls. qPCR reaction samples were prepared as follows: 4 μL of the diluted cDNA (10 ng in total) were mixed with 5 μL of SYBR green (TAKYON, Eurogentec, Liege, Belgium) and 0.5 μL of each primer (4 μM each) in a final volume of 10 μL. Primers used for transcript detection

Table 1. Primers used for RT-qPCR

	Forward	Reverse
SOX2	AGTCTCCAAGCGACGAAAAA	TTTCACGTTTGCAACTGTCC
OCT7	CTGACGATCTCCACGCAGTA	GGCAGAAAGCTGTCCAAGTC
SALL2	ACTCCTCTGGGGTGACCTTT	GGAGTGGTAGTGGAGGTGGA
Intα6	TTCCTGTTTCCTAGCTGTGT	ACTCTTTGGCCTGTTAGTCA
CD44	TCCAACACCTCCCAGTATGACA	GGCAGGTCTGTGACTGATGTACA
18S	AACTTTCGATGGTATCGCCG	CCTTGGATGTGGTAGCCGTTT
hTBP	ACAGCCTGCCACCTTACG	TGCCATAAGGCATCATTGGACTA

are described in Table 1. RT-qPCR was performed using the Roche LightCycler 480 (3 min at 95°C of activation; 45 cycles: denaturation 95°C, 3 s, hybridization and elongation 60°C 25 s).

Flow cytometry

Tumorspheres or cells cultured as monolayers were washed with PBS and dissociated by incubation during 10 min at 37°C with Accutase or trypsin-EDTA (Biowest), respectively, then centrifuged (350*g*, 5 min, 4°C), and washed with flow buffer. 5 μL of APC-conjugated anti-CXCR4 (1/20; BioLegend, Amsterdam, the Netherlands) or BV421-conjugated anti-CD133 antibody (1/25; BioLegend, Amsterdam, the Netherlands) was added to 1×10^5 cells in 100 μL of flow buffer and kept at 4°C for 1 h in the dark. Cells were then washed and centrifuged at 400*g* for 4 min at 4°C. After a second wash, cells were resuspended in 200 μL of flow buffer and analyzed with the FACSCanto II (BD Biosciences). Data were analyzed with FlowJo software.

Clonogenic assay

GB138 cells were seeded in 6-well plates (400K cells/well) for 24 h. Cells were then mock-infected or infected with oHSV or oHSV/P2G (MOI: 0.1) for 18 h before being harvested and counted. 500 cells were re-seeded in 6-wells plates for 7 days. They were then fixed with paraformaldehyde (4%, 10 min, room temperature [RT]) and stained with crystal violet (10 min, RT). After a final wash, colonies were counted, and the plating efficiency was expressed as the number of colonies/the number of plated cells × 100. Finally, cells were lysed with 0.1% SDS, and crystal violet absorbance was measured to confirm the colonies count.

Tumorspheres assay

GB138 cells were seeded in 6 wells-plates in DMEM HG media + 10% FBS (400,000 cells/well) for 24 h before being infected (MOI: 0.1). T08, T013, T018, and T033 cells were seeded in T25 in stem cell media (250K cells/flask). As spheres reach sufficient size, they were infected (MOI: 0.1). After 18 h of infection, cells were either harvested with trypsin-EDTA or dissociated using Accutase. 125K cells were transferred to a T25 in stem cell media. Alternatively, non-infected cells were seeded (125K cells in a T25) in stem cell media in the presence of conditioned media. Tumorsphere formation efficiency was evaluated after 6 days and expressed as the number of tumorspheres/the number of plated cells × 100.

Migration quantification by transwell assay

The upper chambers of ThinCerts transwells (pore size: 8 μm; Greiner Bio-One, CELLSTAR) placed in a 24-well plate (Greiner Bio-One) were filed with 60 μL of laminin (20 μg/mL in PBS) and incubated for 24 h at 37°C. Excess laminin was removed, 25K cells were plated in a final volume of 200 μL of conditioned media without growth factors, and 300 μL of complete medium were added. After 48 h, the medium was removed, and inserts were washed with PBS. Cells were then fixed with 4% paraformaldehyde for 10 min and washed with PBS, before being stained with crystal violet for 10 min. Non-migrating cells were removed from the transwell with a cotton swab, and invading cells were counted with ImageJ on five pictures taken randomly (magnification X20). The percentage of migrating cells is expressed as the number of invading cells/the number of plated cells × 100.

Sprouting assay

Tumorspheres were either infected with oHSV or oHSV/P2G or cultured with conditioned media for 24 h. They were then seeded into wells of a 96-well plate previously coated with 50 μL hydrobromide poly-D-lysine (10 μg/mL) for 30 min, washed with sterile water, and left to dry overnight under the hood. If infected, tumorspheres were kept in DMEM media without growth factors, while, if pretreated with conditioned media, they were kept in DMEM supplemented with conditioned media (50/50).

Pictures of the tumorspheres were taken with an optical microscope 1 h after plating and after 24 h of incubation. The migration level is measured using ImageJ and expressed as the percentage of migration regarding the tumorspheres area 1 h after plating (*Area at* 24*h-area at* 1*h* * 100).

In vivo experiments

All *in vivo* experiments were performed as previously approved by the Animal Ethical Committee of the University of Liège, in accordance with the Declaration of Helsinki and following the guidelines of the Belgium Ministry of Agriculture in agreement with European Commission Laboratory Animal Care and Use Regulation. Six-week-old female immunodeficient Crl:NU-Foxn1nu mice (Charles River Laboratories, Brussels, Belgium) were used for xenograft experiments. They were housed at the Animal Facility, University of Liège,

in sterilized, filter-topped cages (controlled temperature: 22°C, controlled lighting: 12h day/night). After 1 week acclimatization period, intra-striatal grafts were performed following the previously described procedures.[24] Briefly, 100K GB138-RFP$^+$Luc$^+$ or T033-LRLG cells resuspended in 2 μL of PBS were injected into the right striatum (stereotactic coordinates: 0.5 mm anterior and 2 mm lateral from the bregma and at a depth of 2.5 mm) of mice previously anesthetized with an intraperitoneal injection (intraperitoneal [i.p.]) of a Rompun (Sedativum 2%, Bayer, Brussels, Belgium) and Ketalar (Ketamin 50 mg/mL, Pfizer, Brussels, Belgium) solution (V/V) prepared just before injection. For GB138 RFP$^+$Luc$^+$ experiments, PBS (control) or oncolytic viruses (oHSV or oHSV/P2G; 10^6 PFU in 2μL of PBS) were injected on day 20 within the tumor, under anesthesia, and using the same stereotactic coordinates. For the long-term experiment (Exp 2), a second intratumor injection of PBS, oHSV, or oHSV-P2G was done on day 42. Mice were sacrificed on day 47 (Exp 1 and 2; light-sheet microscopy) or on day 139 (Exp 3, long-term experiment).

For T033-LRLG experiments, treatments were injected on day 14 and 21 and mice were sacrificed on Day 35. One non-treated mouse was sacrificed on day 63 to observe long-term development of T033-LRLG tumors. Mice health status (weight and behavior) was evaluated daily.

ARRIVE 2.0 (Animal Research: Reporting of *In vivo* Experiments) reporting guideline was used to assure the adequate management of animals.[54]

Bioluminescence activity

Mice engrafted with GB138-RFP$^+$Luc$^+$ were injected i.p. with Beetle Luciferin potassium salt (ref. E1605, Promega) (150 mg/kg) and imaged (under 2.5% isoflurane anesthesia) with camera-based bioluminescence imaging system (Xenogen IVIS 50; exposure time 1 min, 15 min after intraperitoneal injection). Regions of interest were defined manually, and images were processed using Living Image and Igor Pro software (version 2.60.1). Raw data were expressed as total counts/min.

Brain tissue clarification and light-sheet microscopy acquisition and analysis

Mice were euthanized with i.p. injection of Euthasol Vet (140 mg/kg), followed by an intracardiac perfusion of ice-cold saline solution. Brains were further clarified to remove lipids and replace them with polyacrylamide. Afterward, brains were incubated for 6 h at RT in 50% RIMS solution (#D2158, Sigma-Aldrich; Refraction index: 1.46; 50% in water). 50% RIMS solution (Refractive Index Matching Solution) was then discarded and replaced by 100% RIMS solution for an overnight incubation at RT.

Eventually, brains were imaged using light-sheet microscopy. Images were acquired with 5X objective (zoom = 0.6; pixel size = 1.52; light-sheet 5.826 μm; center thickness = 12.4; image size = 2,922.4 × 2,922.4 μm^2) and processed to obtain one merged image per plane and 3D reconstruction using Zeiss Arivis software.

Tumors were visualized thanks to the RFP signal while the *corpus callosum* was annotated on each individual image based on the brain autofluorescence signal. Tumor and *corpus callosum* 3D modeling were performed on Imaris Image Analysis software and allowed whole tumor volume and migrating cells volume measurements.

Brain tissue processing and tumor volume measurement

Mice were euthanized with i.p. injection of Euthasol Vet (140 mg/kg) and intracardiac perfusion of ice-cold saline solution, followed by paraformaldehyde 4% in PBS (for histology). Brains were incubated in sucrose 30% (Fisher Chemical; 48 h, 4°C) for tissue cryopreservation, and sectioned into 14 μm-thick serial sections using a cryostat. On a single SuperFrost (Thermo Scientific) adhesive slide, two consecutive brain sections are separated by 420 μm (=14 μm × 30 sections) of tissue thickness, with the 29 intermediate sections distributed across 29 other SuperFrost slides.

Tumor volume analysis was performed either after immunohistochemical staining in the GB138 model or based on the dsRed fluorescence in the T033-LRLG model.

In the GB138 model, tumor cells were detected by immunohistochemical detection of human vimentin (Mouse anti-human vimentin, MAB3400, Merck, 1:200) with PolyviewPlus HRP-DAB kit (Enzo Life Sciences, Brussels, Belgium). The tumor was delineated in QuPath based on anti-human vimentin positivity. On each slide, whole tumor volume was calculated by summing the volumes between consecutive sections, using the truncated cone volume formula: $V = \text{height} \times \pi^3 \times (R1^2 + R2^2 + R1 \times R2)$ where height is the distance between two consecutive slices (420 μm) and R1 and R2 are their radii, determined by treating their areas (μm^2) as circles using the formula: $R = SQRT(Area/\pi)$.

For tumor detection in the T033 model, sections were permeabilized with 0.1% Triton X-100 (VWR) in PBS, and nuclei were counterstained with Hoechst (Sigma-Aldrich). Whole-slide images were acquired using a Zeiss Axioscan 7 slide scanner (20× objective). Tumor cell detection was performed in QuPath using a machine learning-based pixel classifier to identify dsRed$^+$ signal. A 100 × 100 μm grid was overlaid on each image, and all grid elements containing tumor annotations were retained as regions of interest. Tumor area was quantified on each brain section as the cumulative area of all annotated tumor elements on this section. Tumor spread was quantified as the cumulative area of annotated grid elements (10,000 μm^2 × number of elements). To evaluate dispersion, mean distances between the centroids of annotated grid elements were calculated. No volume or 3D reconstruction was attempted for this model because of the absence of a delineated tumor mass.

Statistical analysis

All statistical analyses were performed using GraphPad Prism 10. Data are displayed as mean ± SD or as boxplot with the whiskers representing the minimum and maximum values. When appropriate, normality was evaluated using Shapiro-Wild test. Depending on

the experiments, one-way ANOVAs or Kruskall-Wallis tests were performed as indicated in the figure legends. For *in vivo* experiments 1 and 2 (Figures 5B–5G), statistical significance was analyzed with R to take into consideration the putative experimental bias. R script is available in supplemental material.

DATA AND CODE AVAILABILITY

All original data shown in the figures and supplemental figures are available upon reasonable request.

ACKNOWLEDGMENTS

D.P. and S.G.J. have benefited respectively from a postdoctoral and doctoral fellowship from TELEVIE-FNRS, Belgium. D.M. is a Research Fellow of the FNRS, Belgium. This work was supported by grants from the National Fund for Scientific Research (FNRS, Télévie); the Special Funds of the University of Liège; and the Leon Fredericq Foundation, Liège, Belgium. The authors would like to thank Prof. A. Chiocca (Brigham and Women's Hospital, Boston, MA, USA) for fHsvQuik-1 BAC; C. Desmet (GIGA, University of Liège) for his help for R-statistical analysis; and all the members of the GIGA Viral Vector, Imaging and Flow Cytometry, Genomics platforms, and animal facilities for valuable technical support. We warmly thank Adeline Deward (www.illuminesciences.be) for the graphical abstract.

AUTHOR CONTRIBUTIONS

Conceptualization: D.P., D.M., and S.-D.C. Virus engineering: S.G.J., D.M., and D.P. with the help of L.M. *In vitro* experiments: D.P. and D.M. *In vivo* experiments: D.M. with the help of L.A., L.C., and B.B. Image analysis: D.M. with the help of H.A. Manuscript writing: D.M., D.P., and S.-D.C. Scientific discussions during the project: D.P., D.M., R.B., N.V., L.A., L.M., and S.-D.C. All authors critically reviewed and edited the manuscript. Funding acquisition: S.-D.C. D.P. and D.M. contributed equally as first authors. L.M. and S.-D.C. contributed equally as last authors. All authors approved the final manuscript.

DECLARATION OF INTERESTS

S.G.J. is currently a Postdoctoral Research Fellow at the Brain Tumor Research Center, Massachusetts General Hospital (MGH), Boston, MA, USA.

D.P. is currently a scientist at Janssen Vaccines and Prevention B.V., Leiden, the Netherlands.

DECLARATION OF GENERATIVE AI AND AI-ASSISTED TECHNOLOGIES IN THE WRITING PROCESS

During the preparation of this work, the author(s) used the Pixel Classifier AI-assisted module of QuPath in order to perform semi-automated identification of $dsRed^{+}$ cells based on manual annotations provided by the author(s). Each resulting image was subsequently reviewed and manually corrected by the author(s).

In addition, the author(s) used ChatGPT (OpenAI) to assist in the development of QuPath scripts for the generation of grid elements and the measurement of distances between them. All generated grid elements and corresponding distance measurements were manually checked and validated for each image.

After using these tools, the author(s) reviewed and edited the content as needed and take(s) full responsibility for the content of the published article.

SUPPLEMENTAL INFORMATION

Supplemental information can be found online at https://doi.org/10.1016/j.omton.2025.201083.

REFERENCES

1. Abedi, A.A., Grunnet, K., Christensen, I.J., Michaelsen, S.R., Muhic, A., Møller, S., Hasselbalch, B., Poulsen, H.S., and Urup, T. (2021). A Prognostic Model for Glioblastoma Patients Treated With Standard Therapy Based on a Prospective Cohort of Consecutive Non-Selected Patients From a Single Institution. Front. Oncol. *11*, 597587. https://doi.org/10.3389/fonc.2021.597587.
2. Goenka, A., Tiek, D., Song, X., Huang, T., Hu, B., and Cheng, S.Y. (2021). The many facets of therapy resistance and tumor recurrence in glioblastoma. Cells *10*, 484. https://doi.org/10.3390/cells10030484.
3. Yi, Y., Hsieh, I.Y., Huang, X., Li, J., and Zhao, W. (2016). Glioblastoma stem-like cells: Characteristics, microenvironment, and therapy. Front. Pharmacol. *7*, 477. https://doi.org/10.3389/fphar.2016.00477.
4. Goffart, N., Kroonen, J., Di Valentin, E., Dedobbeleer, M., Denne, A., Martinive, P., and Rogister, B. (2015). Adult mouse subventricular zones stimulate glioblastoma stem cells specific invasion through CXCL12/CXCR4 signaling. Neuro Oncol. *17*, 81–94. https://doi.org/10.1093/neuonc/nou144.
5. Goffart, N., Lombard, A., Lallemand, F., Kroonen, J., Nassen, J., Di Valentin, E., Berendsen, S., Dedobbeleer, M., Willems, E., Robe, P., et al. (2017). CXCL12 mediates glioblastoma resistance to radiotherapy in the subventricular zone. Neuro Oncol. *19*, 66–77. https://doi.org/10.1093/neuonc/now136.
6. Piccirillo, S.G., Spiteri, I., Sottoriva, A., Touloumis, A., Ber, S., Price, S.J., Heywood, R., Francis, N.J., Howarth, K.D., Collins, V.P., et al. (2015). Contributions to drug resistance in glioblastoma derived from malignant cells in the sub-ependymal zone. Cancer Res. *75*, 194–202. https://doi.org/10.1158/0008-5472.CAN-13-3131.
7. Lara-Velazquez, M., Al-Kharboosh, R., Jeanneret, S., Vazquez-Ramos, C., Mahato, D., Tavanaiepour, D., Rahmathulla, G., and Quinones-Hinojosa, A. (2017). Advances in brain tumor surgery for glioblastoma in adults. Brain Sci. *7*, 166. https://doi.org/10.3390/brainsci7120166.
8. Johnson, A.L., Laterra, J., and Lopez-Bertoni, H. (2022). Exploring glioblastoma stem cell heterogeneity: Immune microenvironment modulation and therapeutic opportunities. Front. Oncol. *12*, 995498. https://doi.org/10.3389/fonc.2022.995498.
9. Shi, Y., Riese, D.J., and Shen, J. (2020). The Role of the CXCL12/CXCR4/CXCR7 Chemokine Axis in Cancer. Front. Pharmacol. *11*, 574667. https://doi.org/10.3389/fphar.2020.574667.
10. Gatti, M., Pattarozzi, A., Bajetto, A., Würth, R., Daga, A., Fiaschi, P., Zona, G., Florio, T., and Barbieri, F. (2013). Inhibition of CXCL12/CXCR4 autocrine/paracrine loop reduces viability of human glioblastoma stem-like cells affecting self-renewal activity. Toxicology *314*, 209–220. https://doi.org/10.1016/j.tox.2013.10.003.
11. Richardson, P.J. (2015). CXCR4 and Glioblastoma. Anti Cancer Agents Med. Chem. *16*, 59–74. https://doi.org/10.2174/1871520615666150824153032.
12. Stevenson, C.B., Ehtesham, M., McMillan, K.M., Valadez, J.G., Edgeworth, M.L., Price, R.R., Abel, T.W., Mapara, K.Y., and Thompson, R.C. (2008). CXCR4 expression is elevated in glioblastoma multiforme and correlates with an increase in intensity and extent of peritumoral T2-weighted magnetic resonance imaging signal abnormalities. Neurosurgery *63*, 560–570. https://doi.org/10.1227/01.NEU.0000324896.26088.EF.
13. Isci, D., D'uonnolo, G., Wantz, M., Rogister, B., Lombard, A., Chevigné, A., Szpakowska, M., and Neirinckx, V. (2021). Patient-oriented perspective on chemokine receptor expression and function in glioma. Cancers *14*, 130. https://doi.org/10.3390/cancers14010130.
14. Li, X., Kim, H.J., Yoo, J., Lee, Y., Nam, C.H., Park, J., Lee, S.-T., Kim, T.M., Choi, S.H., Won, J.-K., et al. (2025). Distant origin of glioblastoma recurrence: neural stem cells in the subventricular zone serve as a source of tumor reconstruction after primary resection. Mol. Cancer *24*, 64. https://doi.org/10.1186/s12943-025-02273-2.
15. Alghamri, M.S., Banerjee, K., Mujeeb, A.A., Mauser, A., Taher, A., Thalla, R., McClellan, B.L., Varela, M.L., Stamatovic, S.M., Martinez-Revollar, G., et al. (2022). Systemic Delivery of an Adjuvant CXCR4-CXCL12 Signaling Inhibitor Encapsulated in Synthetic Protein Nanoparticles for Glioma Immunotherapy. ACS Nano *16*, 8729–8750. https://doi.org/10.1021/acsnano.1c07492.
16. Luo, Z., Wang, B., Chen, Y., Liu, H., and Shi, L. (2020). Novel CXCR4 Inhibitor CPZ1344 Inhibits the Proliferation, Migration and Angiogenesis of Glioblastoma. Pathol. Oncol. Res. *26*, 2597–2604. https://doi.org/10.1007/s12253-020-00827-x.
17. Huynh, C., Dingemanse, J., Meyer zu Schwabedissen, H.E., and Sidharta, P.N. (2020). Relevance of the CXCR4/CXCR7-CXCL12 axis and its effect in pathophysiological conditions. Pharmacol. Res. *161*, 105092. https://doi.org/10.1016/j.phrs.2020.105092.
18. Crump, M.P., Gong, J.H., Loetscher, P., Rajarathnam, K., Amara, A., Arenzana-Seisdedos, F., Virelizier, J.L., Baggiolini, M., Sykes, B.D., and Clark-Lewis, I.

(1997). Solution structure and basis for functional activity of stromal cell-derived factor-1; dissociation of CXCR4 activation from binding and inhibition of HIV-1. EMBO J. *16*, 6996–7007. https://doi.org/10.1093/emboj/16.23.6996.

19. Williams, S.A., Harata-Lee, Y., Comerford, I., Anderson, R.L., Smyth, M.J., and McColl, S.R. (2010). Multiple functions of CXCL12 in a syngeneic model of breast cancer. Mol. Cancer *9*, 250. https://doi.org/10.1186/1476-4598-9-250.

20. Neklyudova, O., Arlt, M.J.E., Brennecke, P., Thelen, M., Gvozdenovic, A., Kuzmanov, A., Robl, B., Botter, S.M., Born, W., and Fuchs, B. (2016). Altered CXCL12 expression reveals a dual role of CXCR4 in osteosarcoma primary tumor growth and metastasis. https://doi.org/10.1007/s00432-016-2185-5.

21. Russell, S.J., Peng, K.W., and Bell, J.C. (2012). Oncolytic virotherapy. Nat. Biotechnol. *30*, 658–670. https://doi.org/10.1038/nbt.2287.

22. Kardani, K., Sanchez Gil, J., and Rabkin, S.D. (2023). Oncolytic herpes simplex viruses for the treatment of glioma and targeting glioblastoma stem-like cells. Front. Cell. Infect. Microbiol. *13*, 1206111. https://doi.org/10.3389/fcimb.2023.1206111.

23. Maruyama, Y., Sakurai, A., Noda, S., Fujiwara, Y., Okura, N., Takagi, T., Asano, J., and Honda, F. (2023). Regulatory Issues: PMDA - Review of Sakigake Designation Products: Oncolytic Virus Therapy with Delytact Injection (Teserpaturev) for Malignant Glioma. Oncologist *28*, 664–670. https://doi.org/10.1093/oncolo/oyad041.

24. Kroonen, J., Nassen, J., Boulanger, Y.G., Provenzano, F., Capraro, V., Bours, V., Martin, D., Deprez, M., Robe, P., and Rogister, B. (2011). Human glioblastoma-initiating cells invade specifically the subventricular zones and olfactory bulbs of mice after striatal injection. Int. J. Cancer *129*, 574–585. https://doi.org/10.1002/ijc.25709.

25. Wakimoto, H., Kesari, S., Farrell, C.J., Curry, W.T., Zaupa, C., Aghi, M., Kuroda, T., Stemmer-Rachamimov, A., Shah, K., Liu, T.C., et al. (2009). Human glioblastoma-derived cancer stem cells: Establishment of invasive glioma models and treatment with oncolytic herpes simplex virus vectors. Cancer Res. *69*, 3472–3481. https://doi.org/10.1158/0008-5472.CAN-08-3886.

26. Iannello, A., Debbeche, O., El Arabi, R., Samarani, S., Hamel, D., Rozenberg, F., Heveker, N., and Ahmad, A. (2011). Herpes simplex virus type 1-induced FasL expression in human monocytic cells and its implications for cell death, viral replication, and immune evasion. Viral Immunol. *24*, 11–26. https://doi.org/10.1089/vim.2010.0083.

27. Busillo, J.M., and Benovic, J.L. (2007). Regulation of CXCR4 signaling. Biochim. Biophys. Acta *1768*, 952–963. https://doi.org/10.1016/j.bbamem.2006.11.002.

28. Jackson, M., Hassiotou, F., and Nowak, A. (2015). Glioblastoma stem-like cells: at the root of tumor recurrence and a therapeutic target. Carcinogenesis *36*, 177–185. https://doi.org/10.1093/carcin/bgu243.

29. Shaheen, S., Ahmed, M., Lorenzi, F., and Nateri, A.S. (2016). Spheroid-Formation (Colonosphere) Assay for in Vitro Assessment and Expansion of Stem Cells in Colon Cancer. Stem Cell Rev. Rep. *12*, 492–499. https://doi.org/10.1007/s12015-016-9664-6.

30. Volovetz, J., Berezovsky, A.D., Alban, T., Chen, Y., Lauko, A., Aranjuez, G.F., Burtscher, A., Shibuya, K., Silver, D.J., Peterson, J., et al. (2020). Identifying conserved molecular targets required for cell migration of glioblastoma cancer stem cells. Cell Death Dis. *11*, 152. https://doi.org/10.1038/s41419-020-2342-2.

31. Lombard, A., Isci, D., Reuter, G., Di Valentin, E., Hego, A., Martin, D., Rogister, B., and Neirinckx, V. (2024). Development of an intraventricular adeno-associated virus-based labeling strategy for glioblastoma cells nested in the subventricular zone. Neurooncol. Adv. *6*, vdae161. https://doi.org/10.1093/noajnl/vdae161.

32. Lombard, A., Digregorio, M., Delcamp, C., Rogister, B., Piette, C., and Coppieters, N. (2020). The Subventricular Zone, a Hideout for Adult and Pediatric High-Grade Glioma Stem Cells. Front. Oncol. *10*, 614930. https://doi.org/10.3389/fonc.2020.614930.

33. Würth, R., Bajetto, A., Harrison, J.K., Barbieri, F., and Florio, T. (2014). CXCL12 modulation of CXCR4 and CXCR7 activity in human glioblastoma stem-like cells and regulation of the tumor microenvironment. Front. Cell. Neurosci. *8*, 144. https://doi.org/10.3389/fncel.2014.00144.

34. Ongprakobkul, N., Ishida, Y., Hatano-Sato, K., Li, K., Petdachai, S., Usumi-Fujita, R., Hosomichi, J., Mahatumarat, K., and Ono, T. (2022). Effects of local vs systemic administration of CXCR4 inhibitor AMD3100 on orthodontic tooth movement in rats. Am. J. Orthod. Dentofacial Orthop. *162*, 182–192. https://doi.org/10.1016/j.ajodo.2021.03.018.

35. Xiong, Y., Sun, M., Yang, Q., Zhang, W., Song, A., Tan, Y., Mao, J., Liu, G., and Xue, P. (2025). Nanoparticle-based drug delivery systems to modulate tumor immune response for glioblastoma treatment. Acta Biomater. *194*, 38–57. https://doi.org/10.1016/j.actbio.2025.01.050.

36. Gregory, J.V., Kadiyala, P., Doherty, R., Cadena, M., Habeel, S., Ruoslahti, E., Lowenstein, P.R., Castro, M.G., and Lahann, J. (2020). Systemic brain tumor delivery of synthetic protein nanoparticles for glioblastoma therapy. Nat. Commun. *11*, 5687. https://doi.org/10.1038/s41467-020-19225-7.

37. Wei, R., Li, J., Lin, W., Pang, X., Yang, H., Lai, S., Wei, X., Jiang, X., Yuan, Y., and Yang, R. (2024). Nanoparticle-mediated blockade of CXCL12/CXCR4 signaling enhances glioblastoma immunotherapy: Monitoring early responses with MRI radiomics. Acta Biomater. *177*, 414–430. https://doi.org/10.1016/j.actbio.2024.02.007.

38. Gratpain, V., Mwema, A., Labrak, Y., Muccioli, G.G., van Pesch, V., and des Rieux, A. (2021). Extracellular vesicles for the treatment of central nervous system diseases. Adv. Drug Deliv. Rev. *174*, 535–552. https://doi.org/10.1016/j.addr.2021.05.006.

39. Ehtesham, M., Winston, J.A., Kabos, P., and Thompson, R.C. (2006). CXCR4 expression mediates glioma cell invasiveness. Oncogene *25*, 2801–2806. https://doi.org/10.1038/sj.onc.1209302.

40. Hira, V.V.V., Breznik, B., Vittori, M., Loncq de Jong, A., Mlakar, J., Oostra, R.-J., Khurshed, M., Molenaar, R.J., Lah, T., and Van Noorden, C.J.F. (2020). Similarities Between Stem Cell Niches in Glioblastoma and Bone Marrow: Rays of Hope for Novel Treatment Strategies. J. Histochem. Cytochem. *68*, 33–57. https://doi.org/10.1369/0022155419878416.

41. Hira, V.V.V., Van Noorden, C.J.F., and Molenaar, R.J. (2020). CXCR4 antagonists as stem cell mobilizers and therapy sensitizers for acute myeloid leukemia and glioblastoma? Biology *9*, 31. https://doi.org/10.3390/biology9020031.

42. Lemos de Matos, A., Franco, L.S., and McFadden, G. (2020). Oncolytic Viruses and the Immune System: The Dynamic Duo. Mol. Ther. Methods Clin. Dev. *17*, 349–358. https://doi.org/10.1016/j.omtm.2020.01.001.

43. Benencia, F., Courrèges, M.C., Conejo-García, J.R., Mohamed-Hadley, A., Zhang, L., Buckanovich, R.J., Carroll, R., Fraser, N., and Coukos, G. (2005). HSV oncolytic therapy upregulates interferon-inducible chemokines and recruits immune effector cells in ovarian cancer. Mol. Ther. *12*, 789–802. https://doi.org/10.1016/j.ymthe.2005.03.026.

44. Ribas, A., Dummer, R., Puzanov, I., VanderWalde, A., Andtbacka, R.H.I., Michielin, O., Olszanski, A.J., Malvehy, J., Cebon, J., Fernandez, E., et al. (2017). Oncolytic Virotherapy Promotes Intratumoral T Cell Infiltration and Improves Anti-PD-1 Immunotherapy. Cell *170*, 1109–1119.e10. https://doi.org/10.1016/j.cell.2017.08.027.

45. D'Alterio, C., Buoncervello, M., Ieranò, C., Napolitano, M., Portella, L., Rea, G., Barbieri, A., Luciano, A., Scognamiglio, G., Tatangelo, F., et al. (2019). Targeting CXCR4 potentiates anti-PD-1 efficacy modifying the tumor microenvironment and inhibiting neoplastic PD-1. J. Exp. Clin. Cancer Res. *38*, 432. https://doi.org/10.1186/s13046-019-1420-8.

46. Zeng, Y., Li, B., Liang, Y., Reeves, P.M., Qu, X., Ran, C., Liu, Q., Callahan, M.V., Sluder, A.E., Gelfand, J.A., et al. (2019). Dual blockade of CXCL12-CXCR4 and PD-1–PD-L1 pathways prolongs survival of ovarian tumor–bearing mice by prevention of immunosuppression in the tumor microenvironment. FASEB J. *33*, 6596–6608. https://doi.org/10.1096/fj.201802067RR.

47. Wu, A., Maxwell, R., Xia, Y., Cardarelli, P., Oyasu, M., Belcaid, Z., Kim, E., Hung, A., Luksik, A.S., Garzon-Muvdi, T., et al. (2019). Combination anti-CXCR4 and anti-PD-1 immunotherapy provides survival benefit in glioblastoma through immune cell modulation of tumor microenvironment. J. Neuro Oncol. *143*, 241–249. https://doi.org/10.1007/s11060-019-03172-5.

48. Jayasingam, S.D., Citartan, M., Thang, T.H., Mat Zin, A.A., Ang, K.C., and Ch'ng, E.S. (2019). Evaluating the Polarization of Tumor-Associated Macrophages Into M1 and M2 Phenotypes in Human Cancer Tissue: Technicalities and Challenges in Routine Clinical Practice. Front. Oncol. *9*, 1512. https://doi.org/10.3389/fonc.2019.01512.

49. Fortunato, O., Belisario, D.C., Compagno, M., Giovinazzo, F., Bracci, C., Pastorino, U., Horenstein, A., Malavasi, F., Ferracini, R., Scala, S., et al. (2020). CXCR4 Inhibition Counteracts Immunosuppressive Properties of Metastatic NSCLC Stem Cells. Front. Immunol. *11*, 02168. https://doi.org/10.3389/fimmu.2020.02168.

50. Todo, T., Martuza, R.L., Rabkin, S.D., and Johnson, P.A. (2001). Oncolytic herpes simplex virus vector with enhanced MHC class I presentation and tumor cell killing. Proc. Natl. Acad. Sci. USA *98*, 6396–6401. https://doi.org/10.1073/pnas.101136398.

51. Tischer, B.K., Kaufer, B.B., Sommer, M., Wussow, F., Arvin, A.M., and Osterrieder, N. (2007). A self-excisable infectious bacterial artificial chromosome clone of varicella-zoster virus allows analysis of the essential tegument protein encoded by ORF9. J. Virol. *81*, 13200–13208. https://doi.org/10.1128/JVI.01148-07.

52. Goins, W.F., Huang, S., Hall, B., Marzulli, M., Cohen, J.B., and Glorioso, J.C. (2020). Engineering HSV-1 Vectors for Gene Therapy. Methods Mol. Biol. *2060*, 73–90. https://doi.org/10.1007/978-1-4939-9814-2_4.

53. Marconi, P., and Manservigi, R. (2014). Herpes simplex virus growth, preparation, and assay. Methods Mol. Biol. *1144*, 19–29. https://doi.org/10.1007/978-1-4939-0428-0_2.

54. Percie du Sert, N., Hurst, V., Ahluwalia, A., Alam, S., Avey, M.T., Baker, M., Browne, W.J., Clark, A., Cuthill, I.C., Dirnagl, U., et al. (2020). The ARRIVE guidelines 2.0: Updated guidelines for reporting animal research. PLoS Biol. *18*, e3000410. https://doi.org/10.1371/journal.pbio.3000410.